HHS Public Access

Author manuscript

Reproduction. Author manuscript; available in PMC 2019 June 01.

Published in final edited form as:

Reproduction. 2018 June ; 155(6): 553–562. doi:10.1530/REP-18-0089.

Radiation-induced ovarian follicle loss occurs without overt stromal changes

Bruce F. Kimler[1], **Shawn M. Briley**[2], **Brian W. Johnson**[3], **Austin G. Armstrong**[2], **Susmita Jasti**[2], and **Francesca E. Duncan**[2,4,*]

[1]Department of Radiation Oncology, University of Kansas Medical Center, Kansas City, KS

[2]Department of Anatomy and Cell Biology, University of Kansas Medical Center, Kansas City, KS

[3]Department of Comparative Medicine, University of Washington, Seattle, WA

[4]Department of Obstetrics and Gynecology, Feinberg School of Medicine, Northwestern University, Chicago, IL

Abstract

Radiation damage due to total body irradiation (TBI) or targeted abdominal radiation can deplete ovarian follicles and accelerate reproductive aging. We characterized a mouse model of low dose TBI to investigate how radiation affects the follicular and stromal compartments of the ovary. A single TBI dose of either 0.1 Gy or 1 Gy (Cesium-137γ) was delivered to reproductively adult CD1 female mice, and sham-treated mice served as controls. Mice were sacrificed either 2 weeks or 5 weeks post-exposure, and ovarian tissue was harvested. To assess the ovarian reserve, we classified and counted the number of morphologically normal follicles in ovarian histologic sections for all experimental cohorts using an objective method based on immunohistochemistry for an oocyte-specific protein (MSY2). 0.1 Gy did not affect that total number of ovarian follicles, whereas 1 Gy resulted in a dramatic loss. At two weeks, there was a significant reduction in all preantral follicles, but early antral and antral follicles were still present. By five weeks, there was complete depletion of all follicle classes. We examined stromal quality using histologic stains to visualize ovarian architecture and fibrosis and by immunohistochemistry and quantitative microscopy to assess cell proliferation, cell death, and vasculature. There were no differences in the ovarian stroma across cohorts with respect to these markers, indicating that this compartment is more radio-resistant relative to the germ cells. These findings have implications for reproductive health and the field of fertility preservation because the radiation doses we examined mimic scatter doses experienced in typical therapeutic regimens.

Keywords

radiation; follicle; stroma; iatrogenic; reproductive aging

[*]**Correspondence:** Francesca E. Duncan, PhD, Department of Obstetrics and Gynecology, Feinberg School of Medicine, Northwestern University, 303 E. Superior Street, Lurie 7-117, Chicago, IL 60611, Tel: 312-503-2172, f-duncan@northwestern.edu.

Declaration of Interest

The authors have no conflict of interest to report.

Introduction

Radiation is a mainstay of treatment for most cancers, and total body irradiation (TBI) is used as a conditioning treatment for bone marrow transplantation. Despite the ability of radiation to target cancer cells, it can also have unintended off-target and long-term consequences on other organ systems. The extent of radiation-induced tissue damage is largely dependent on factors such as patient age, treatment dose and regimen, and radiation field (Meirow, et al. 2010). Radiation can negatively impact all aspects of the female reproductive axis. For example, radiation directed to the cranium can damage the hypothalamus and pituitary leading to altered neuroendocrine function (Wo and Viswanathan 2009). Radiation exposure to the uterus can decrease uterine weight and size, impair endometrial thickening, and disrupt the vasculature and blood flow (Critchley and Wallace 2005). Such uterine alterations can increase the risk of miscarriage, placental abnormalities, preterm birth, and delivery of low birth weight offspring (Wo and Viswanathan 2009).

The ovary is particularly susceptible to radiation damage, with the dose required to eliminate half the primordial follicles in the ovary estimated at 2 Gy (Wallace, et al. 2003). The follicle is the functional unit of the ovary and consists of a germ cell surrounded by supporting somatic cells. Follicles produce endocrine hormones and are essential for generating mature gametes capable of being fertilized. Thus, the number of follicles within the ovary is an important readout of reproductive function. Females are born with a finite number of primordial follicles which dictate the ovarian reserve and reproductive lifespan. During physiologic reproductive aging, the number of follicles within the ovary steadily declines through processes of recruitment and cell death, such that females are born with approximately 1 million primordial follicles but end up with only about 1,000 at the time of menopause (Broekmans, et al. 2009). Factors such as radiation accelerate reproductive aging. Importantly, there is no evidence of follicular renewal following radiation-induced depletion, and thus, exposure can result in premature ovarian failure, subfertility, and infertility (Kerr, et al. 2012a). In fact, ovarian failure has been reported in 90% of females who received TBI and in 97% of those who received abdominal radiation (Sanders, et al. 1996, Wallace, et al. 1989). Therefore, understanding the cellular and molecular mechanisms that underlie radiation-induced ovarian damage has important implications for reproductive health.

To date, a significant amount of research has pinpointed DNA damage checkpoints and intrinsic apoptosis pathways as critical regulators of radiation-induced cell death within the oocyte (Hutt 2014, Kerr, et al. 2012b, Rinaldi, et al. 2017). In fact, genetic and pharmacologic manipulations of these pathways have been harnessed for fertoprotection efforts to preserve germ cells and endocrine function in response to radiation damage (Morita, et al. 2000, Rinaldi, et al. 2017, Zelinski, et al. 2011). However, less is known about the effect of radiation on the ovarian microenvironment especially in response to low doses of radiation that are known to affect the follicle. The ovarian microenvironment consists of the stroma, or a mixture of extracellular matrix components as well as theca-interstitial, immune, endothelial, and smooth muscle cells. The ovarian stroma provides the physical and signaling milieu in which follicles grow and develop. Thus, damage to the stroma can have

important long-term ramifications on germ cell health and reproductive function. In this study we characterized the simultaneous effect of low dose radiation exposure on both the follicular and stromal components of the ovary in a reproductively mature animal model of TBI.

Materials and Methods

Animals, irradiation paradigm, and ovarian tissue harvesting

CD1 female mice were obtained from Envigo (Indianapolis, IN) and were housed in a controlled barrier facility at the University of Kansas Medical Center's (KUMC) Research Support Facility under constant temperature, humidity, and light (12h light/12h dark). Food and water were provided *ad libitum*. All experimental protocols were approved by the Institutional Animal Care and Use Committee of the University of Kansas Medical Center and were in accordance with National Institutes of Health Guidelines.

At 6 weeks of age, mice were exposed to a single dose of 0.1 Gy or 1 Gy total body irradiation using a Model MK I-68 Cesium-137 Irradiator (J L Shepherd and Associates, San Fernando, CA) (Supplemental Figure 1). A 302 shaped attenuator was used to produce a uniform field and a dose rate of 2.1 Gy/min. A 10× attenuator was added for the low dose irradiation. With these conditions, all irradiations took 48 seconds per mouse. During this time, the mice were confined to standardize exposure. Sham-treated mice served as controls. These mice were handled in the same manner as the experimental cohorts but were not exposed to radiation. Following irradiation, mice were group housed in sterile cages.

Animals in each cohort (0.1 Gy, 1 Gy, Sham) were euthanized either 2 or 5 weeks post-irradiation and ovarian tissue was harvested (Supplemental Figure 1). Ovaries were fixed in Modified Davidson's (Electron Microcopy Sciences, Hatfield, PA) for 6 hours at room temperature and then overnight at 4°C. After fixation, these ovaries were dehydrated using an automated tissue processor (Leica Biosystems, Buffalo Grove, IL), embedded in paraffin, and serially sectioned (5 μm thickness). For all experiments described below, ovarian tissue from a minimum of 3 animals per cohort was examined and representative images were analyzed and are shown.

Follicle identification and counting

Follicles were counted in every 5^{th} section throughout each ovary according to previously published protocols (Bristol-Gould, et al. 2006, Duncan, et al. 2017). Follicle stages were classified according to morphological criteria, and only healthy follicles were counted (Duncan, et al. 2017). Primordial follicles were classified as an oocyte surrounded by squamous granulosa cells, whereas primary follicles were characterized as oocytes surrounded by a complete single layer of cuboidal granulosa cells. All primordial and primary follicles were counted irrespective of whether the oocyte nucleus was visible in the section. Secondary follicles contained a larger oocyte surrounded by more than one layer of granulosa cells. Early antral follicles contained a developing antral cavity, and antral follicles were the largest follicles with prominent antral spaces. For secondary through antral stages, only follicles with an oocyte nucleus present in the section were counted to avoid

double counting. The total follicle count for each stage per ovary was then divided by the total number of sections counted per ovary to obtain an average number of follicles per section.

The objectivity of the follicle counting procedure was enhanced by performing immunohistochemistry on sections used for follicle counting with an antibody against the oocyte-specific marker MSY-2 (generous gift of Dr. Richard M. Schultz, University of Pennsylvania). Only follicles containing MSY2-positive oocytes were counted. In brief, slides were deparaffinized in Citrisolv (Thermo Fisher, Waltham, MA) and rehydrated in a series of graded ethanol baths (100%, 95%, 85%, 70% and 50%). Antigen retrieval was performed by microwaving slides in 1× Reveal Decloaker (BioCare Medical, Pacheco, CA) at 50% power for two minutes followed by 10% power for seven minutes. Slides were washed with Tris-Buffered Saline supplemented with 0.1% Tween-20 (TBST) twice for 15 minutes and then incubated in 3% hydrogen peroxide for 15 minutes at room temperature. Slides were briefly rinsed in Tris-Buffered Saline (TBS) and blocked using the Avidin/Biotin blocking kit (Vector Laboratories, Burlingame, CA). The slides were briefly rinsed with TBS and the area around the tissue was defined using a PAP pen. The slides were incubated in blocking buffer (10% normal goat serum, 0.3% Triton X-100 in TBS) for one hour. The blocking buffer was removed and the slides were incubated in primary antibody diluted in blocking buffer (1:4000) overnight at 4°C. Slides were then rinsed three times in TBST for 5 minutes each. Secondary antibody incubation and horseradish peroxidase (HRP) conjugation was performed using the VECTASTAIN Elite ABC HRP Kit according to the provided instructions. Detection was performed using 3,3′-diaminobenzidine (DAB) using the DAB Peroxidase (HRP) Substrate Kit according to the manufacturer's instructions (Vector Laboratories). The reaction was allowed to proceed for 1 minute. Counterstaining was performed as follows: 1 minute incubation in hematoxylin, 2 minutes in running water, 20 seconds in acid ethanol, running water for 1 minute, hematoxylin for 1 minute, a brief rinse in water, bluing reagent for 1 minute and running water for one minute. The slides were then dehydrated in graded ethanol baths (80%, 95% and 100%), cleared in Citrisolv, and mounted with Cytoseal.

Histologic staining

Ovarian histologic sections from each animal in all experimental cohorts were stained with Hematoxylin and Eosin (H&E), Periodic Acid Schiff (PAS), and Picrosirus Red (PSR) as previously described (Briley, et al. 2016). To view entire ovary sections, individual 40× brightfield images were taken and stitched together using an EVOS FL Auto Cell Imaging system (Thermo Fisher).

Automated immunohistochemistry and quantitative microscopy

We performed automated immunohistochemistry through the University of Washington Histology and Imaging Core (UW-HIC) with antibodies specific to Ki67 (Clone D3B5, Cell Signaling, Danvers, MA), cleaved caspase 3 (CC3, BioCare Medical), and CD31 (Clone SZ31, Dianova, Hamburg, Germany) to assess proliferation, apoptosis, and vasculature, respectively, in ovarian histologic sections from all experimental cohorts. In brief, Slides were baked for 30 minutes at 60°C and deparaffinized on the Leica Bond MAX Automated

Immunostainer (Leica Microsystems, Buffalo Grove, IL) using Leica Bond Dewax Solution (Leica Cat No. AR922). Antigen retrieval was performed on all slides using EDTA solution pH 9.0 (Lieca Bond Epitope Retrieval Solution 2, Cat No AR9640) at 100°C for 10 or 20 minutes depending on the antibody used. Blocking consisted of 10% Normal Goat Serum in TBS buffer for 20 minutes at room temperature. The primary antibodies were diluted as follows in Leica Bond Primary Antibody Diluent (Leica Cat No. AR9352): Ki67 (1:400), CC3 (1:100), and CD31 (1:50). Slides were incubated with Ki-67 and CD31 primary antibodies for 30 minutes at room temperature. Remaining slides were incubated with CC3 antibody for 60 minutes at room temperature. Slides probed with CD31 primary antibody were then incubated with unconjugated Rabbit Anti-Rat IgG (H+L), mouse adsorbed, secondary antibody for 8 minutes at room temperature. All slides were incubated with goat anti-rabbit poly-HRP polymerized secondary detection (Leica Cat No DS9800) for 8 minutes at room temperature. Additional blocking for endogenous peroxidase was then performed using Leica peroxide block (3% H2O2/Leica Cat No DS9800) for 5 minutes at room temperature. Sections were then incubated with Leica Bond Mixed Refine DAB substrate detection for 10 minutes at room temperature. (Leica Cat No DS9800). Antibody complexes were visualized using Leica Bond Mixed Refine (DAB, 3,3′-diaminobenzidine) detection 2× for 10 minutes at RT (Leica Cat No DS9800). Tissues were counterstained with hematoxylin counterstain for 4 minutes followed by two rinses in water. Slides were then dehydrated through 100% ETOH, cleared in Xylene and mounted with synthetic resin mounting medium and a #1.5 coverslip.

Slides were scanned in brightfield with a 20× objective using the Hamamatsu NanoZoomer Digital Pathology System HT9600, (Hamamatsu City, Japan). The digital images were then imported into Visiopharm software (Hoersholm, Denmark) for analysis. Using the Visiopharm Image Analysis module, three regions of interests (ROI) were manually drawn around the follicles, corpora lutea, and the stroma respectively. In addition, the entire area of the ovary was determined. Follicles were identified as the functional units of the ovary containing an oocyte surrounded by layers of granulosa cells all contained within a visible basement membrane. Corpora lutea were identified based on the morphology of luteinized cells which have a characteristic hypertrophied and eosinophilic appearance relative to non-luteinized granulosa and theca cells (Supplemental Figure 4D). Of note, we only classified structures as corpora lutea if there was a clear boundary enclosing the luteinized cells. Thus, it is likely that degrading corpora lutea from previous cycles were considered as interstitial stromal cells. The stromal area was defined as the total ovarian area minus the sum of the total follicular area and the total corpora lutea area. By converting the initial digital image into grayscale values using two features, HDAB – HDAB and RGB – B, the Visiopharm software was trained to label positive staining (DAB) and background tissue counterstain (hematoxylin) using a project specific configuration based on a threshold of pixel values. The images were processed in batch mode using this configuration to generate the desired per area outputs and analyzed at 100%. Ovarian histologic sections from each animal in all experimental cohorts were analyzed.

Statistical analysis

Significant changes between groups were analyzed by one-way ANOVA or two-way ANOVA followed by multiple comparisons test. P values < 0.05 were considered statistically significant. Statistical analysis was performed using Graphpad-Prism Software Version 6.0f (La Jolla, CA).

Results

TBI depletes ovarian follicles in a dose-dependent manner

To examine how ovarian follicles respond to low doses of radiation, we established an adult animal model of TBI (Supplemental Figure 1). Reproductively adult CD1 female mice were exposed to a single dose of either 0.1 Gy or 1 Gy of γ radiation delivered uniformly to the whole body. Ovaries were then harvested either 2 or 5 weeks post-exposure, and follicles were classified by stage according to morphology and quantified. Typically, follicles are evaluated in hematoxylin and eosin (H&E) stained histologic sections, but this method is subjective especially when trying to identify small primordial follicles in the ovarian cortex (Supplemental Figure 2A–B). To improve the objectivity of follicle counting, we immunostained ovarian histologic sections using an antibody against MSY-2, an abundant oocyte-specific protein that localizes to the cytoplasm (Supplemental Figure 2C–D)(Yu, et al. 2002). This marker clearly delineated oocytes and improved the ability to identify and quantify follicles relative to sections that were stained with H&E alone (Supplemental Figure 2).

Using this follicle detection strategy, we determined that a single dose exposure to 0.1 Gy radiation did not cause a significant decrease in the number of follicles. At 2 weeks post-irradiation, average follicle counts were 33.2 ± 2.2 follicles/section in irradiated mice compared to 43.6 ± 8.5 follicles/section in sham-treated age-matched mice, but this change was not significant (Figure 1A, B, G). At 5 weeks post-irradiation, the average number of follicles per section was 22.4 ± 1.2 in irradiated mice compared to 33.1 ± 3.0 in the controls, and again this difference was not significant (Figure 1D, E, G). In contrast to 0.1 Gy radiation, 1 Gy radiation caused a significant depletion of follicles compared to controls at both the 2 and 5 week time points (Figure 1C, F, and G). Post-exposure to 1 Gy radiation, there were only 1.6 ± 0.1 follicles/section at 2 weeks and no follicles remaining at 5 weeks (Figure 1G). This average follicle number was also significantly less than that observed in the ovaries from 0.1 Gy-exposed mice at both time points (Figure 1G). These findings demonstrate that in adult CD1 mice, exposure to γ radiation causes a dose-dependent reduction in the total number of ovarian follicles with 1 Gy causing significantly more damage compared to 0.1 Gy.

A single dose exposure to 1 Gy TBI differentially affects follicle classes

Although 1 Gy exposure caused a significant reduction in total follicle numbers relative to ovaries from mice that were exposed to 0.1 Gy radiation or sham controls, histologic evaluation demonstrated that the follicle classes affected were different between the 2 and 5 week time points (Figures 2–3). Ovaries from mice that received a single dose of 1 Gy radiation lacked primordial follicles in the ovarian cortex at both 2 and 5 weeks post-

exposure, and this was in contrast to mice exposed to 0.1 Gy radiation and sham controls which all showed evidence of primordial follicles (Figure 2). However, whereas no follicles were present in ovaries from 1 Gy-exposed mice following 5 weeks post-treatment, large growing follicles were still visible at 2 weeks (Figures 2C and F).

To further quantify these phenotypes, we performed follicle counts across different classes and normalized counts to the sham control (Figure 3). At 2 weeks post-exposure, 1 Gy radiation completely eliminated both primordial and primary follicles and significantly reduced the number of secondary follicles relative to mice exposed to 0.1 Gy radiation or sham controls (Figure 3A). There were no differences in the number of early antral follicles between the experimental cohorts, and there was even an increase in the number of antral follicles in mice exposed to 1 Gy radiation relative to both 0.1 Gy and the sham control (Figure 3A). In contrast and consistent with the histology, 1 Gy radiation completely eradicated all follicle classes at 5 weeks post-exposure relative to both 0.1 Gy and the sham control, and there were no differences across the follicle classes in the 0.1 Gy and sham cohorts (Figure 3B). Taken together, these results demonstrate that 1 Gy radiation rapidly eliminates the majority of dormant and early growing follicles in the ovary, but that a subset of follicles can survive and grow to antral stages following short-term exposure.

The ovarian stroma is resistant to doses of TBI that are sufficient to deplete ovarian follicles

To investigate how the ovarian stroma was affected by the same dose of radiation that significantly damaged the ovarian reserve, we performed a histologic analysis of ovaries from mice that were treated with 1 Gy radiation and harvested 2 and 5 weeks post-exposure (Figure 4). We stained ovarian tissue sections with hematoxylin and eosin (H&E) to evaluate general tissue morphology (Figures 4A–D). We did not observe obvious gross morphological differences across cohorts except for the complete absence of follicles in ovaries from mice that were harvested at 5 weeks post-exposure (Figure 4D). Interestingly, the remaining tissue in these ovarian sections had a luteinized appearance characterized by eosinophilic and hypertrophied cells analogous to the corpora lutea in the other experimental cohorts (Figure 4A–D). We also stained sections with Periodic Acid Schiff (PAS) which detects polysaccharides. We previously used PAS to visualize multinucleated macrophage giant cells in fibrotic ovarian tissue from mice of advanced reproductive age (Briley, et al. 2016). However, here we did not observe any differences in PAS staining across experimental cohorts (Figures 4E–H). Finally, we stained sections with Pircosirius Red (PSR), a histologic stain specific for collagen I and III, which is often used to detect fibrosis (Briley, et al. 2016). We did not observe prominent differences in PSR staining among ovaries from the different experimental cohorts suggesting that radiation exposure did not induce ovarian fibrosis. Not surprisingly, we also did not observe differences in H&E, PAS, and PSR staining in ovaries from mice exposed to 0.1 Gy radiation relative to sham controls at either the 2 week or 5 week time points (Supplemental Figure 3).

To further examine how low dose exposure to radiation affects the ovarian stroma, we optimized and validated automated immunohistochemistry protocols on ovarian tissue sections for two markers of general tissue health, including Ki67 for proliferating cells and

cleaved caspase 3 (CC3) for apoptotic cells (Supplemental Figures 4A–B). Ki67 refers to the antigen recognized by a monoclonal antibody that was generated by immunizing mice with nuclei of a Hodgkin lymphoma cell line (Scholzen and Gerdes 2000). Although the exact function of this protein remains elusive, it is expressed in nuclei of cells in G1, S, G2, and M phases but not in resting cells and, therefore, is commonly used as a proliferation marker (Scholzen and Gerdes 2000). On the other hand, CC3 is an effector caspase involved in the initiation of the cell death pathway and is often used as a marker of cellular apoptosis (Nicholson, et al. 1995). Using quantitative immunohistochemistry approaches, we analyzed Ki67 and CC3 staining in ovarian tissue sections across experimental cohorts in specific compartments of the ovarian tissue (follicles, corpora lutea, and stroma) and quantified the number of cells positive for each marker (Figures 5A–C). In general, more proliferative (Ki67 positive) and apoptotic cells (CC3 positive) were observed in follicles relative to the corpora lutea and stroma (Figure 5D–I). There was an increase in the number of proliferating cells in follicles from the sham cohort between the 2 week and 5 week time point (Figure 5A). In addition, at the 2 week time point, there was an increase in the number of proliferating cells in follicles following exposure to 1 Gy radiation relative to the sham controls, consistent with the preservation and increase in early antral and antral follicles, respectively, in the 1 Gy cohort (Figures 3A and 5A). Proliferating follicle cells were obviously not observed at 5 weeks in the 1 Gy cohort due to the complete depletion of follicles (Figures 1G, 3B, and 5D). No differences in proliferation were observed across experimental cohorts in the corpora lutea or the stroma (Figures 5E–F). Moreover, the number of apoptotic cells did not change irrespective of treatment in any of the ovarian compartments (Figures 5G–I).

We also examined the architecture of the ovarian vasculature by performing immunohistochemistry with an antibody against CD31, a membrane glycoprotein that is expressed at high levels in early and mature endothelial cells (Figure 6). Based on our histologic analysis, the CD31 staining pattern in the ovary was similar across the experimental cohorts and localized as expected. For example, in groups where growing follicles were still present in the tissue, the vasculature was prominent in the theca layer surrounding the follicles. In all groups, corpora lutea were visible in the histologic sections and were highly vascularized. The stromal and interstitial vessels were also similar across cohorts.

Discussion

In a sexually mature mouse model of TBI, we report a clear dose response of ovarian follicles to ionizing radiation. To increase the objectivity and accuracy of follicle counting, we quantified follicle numbers in ovarian histologic sections by performing immunohistochemistry for an oocyte-specific marker. Using this method, we demonstrated that 1.0 Gy radiation caused a significant reduction in total follicle numbers at both 2 weeks and 5 weeks post-exposure, whereas there was no such significant reduction in response to 0.1 Gy radiation at either time point. These results are in contrast to another study that showed a near complete destruction of primordial follicles at 2 weeks following a single dose exposure of 0.1 Gy TBI (Morita, et al. 2000). Such inconsistencies underscore the need to consider the numerous variables which can impact the effects of ionizing radiation when

interpreting results, including animal age and strain, oocyte and follicle stage, the experimental design (e.g. radiation dose, rate, exposure, and frequency), and the measured endpoints (Baker 1978). While we used an analogous experimental paradigm as the previous study, they did not report the mouse strain which may account for the observed differences. For example, we used an outbred mouse strain which may be more radio-resistant compared to inbred strains due to their genetic heterogeneity.

In addition to a dose response, we also observed a follicle stage-dependent response to radiation. Early growing follicles from the primordial to secondary stages were significantly depleted in response to 1.0 Gy radiation whereas later stage follicles were still present in either equal or greater numbers relative to sham controls. These findings are consistent with previous mouse and rat data demonstrating that early follicle stages have a high sensitivity to radiation and larger follicles have a low sensitivity (Adriaens, et al. 2009). These persistent larger follicles likely derived from early growing follicles that escaped radiation damage.

In contrast to the changes we observed in ovarian follicles with the experimental paradigm of radiation exposure we used, the surrounding stroma remained unaffected at both doses of radiation based on gross markers of tissue health. In general, quantitative levels of stromal cell proliferation and death, were indistinguishable between irradiated and sham cohorts at both 2 and 5 weeks post-radiation exposure. In human ovaries, radiation exposure not only causes follicle loss, but it is also associated with documented changes in the ovarian stroma including increased cortical fibrosis (Grigsby, et al. 1995). In addition, ionizing radiation can cause vascular damage in many tissues through induction of endothelial cell injury, and in ovaries from women who were treated with a sterilizing dose of radiation, there is an acceleration of spontaneous sclerosis of the ovarian arteries and arterioles (Grigsby, et al. 1995). In our study, we did not detect prominent fibrosis or obvious changes in the ovarian vasculature at any of the radiation doses or time points investigated. This could be because single dose exposures of either 0.1 Gy or 1 Gy ionizing radiation are not sufficient to induce these cellular responses in reproductively adult mice. In addition, it is possible that 5 weeks post-irradiation may be too early a time point to observe chronic effects of radiation exposure. In fact, in humans both radiation-induced vascular injury and tissue fibrosis are both long-term consequences of exposure which can take up to years to manifest clinically (Straub, et al. 2015, Weintraub, et al. 2010). However, the doses of radiation we examined in this study mimic those that occur as scatter doses in typical therapeutic interventions. Thus, in the setting of fertility preservation it will be particularly important to evaluate the functional ability of the radiation-exposed stromal compartment to fully support long-term follicle and gamete development.

Follicle loss is a common feature of both iatrogenic reproductive aging due to radiation and physiologic reproductive aging, and advanced reproductive age is also associated with increased stromal fibrosis (Briley, et al. 2016, Broekmans, et al. 2009, Wallace, et al. 2003). In our model of radiation-induced damage, complete follicle loss was observed in the absence of detectable fibrosis. This observation may provide important insights into the temporal events of ovarian changes that drive physiologic reproductive aging. For example, age-associated fibrosis in the ovary may be a consequence of follicular loss rather than the cause of it. Studies with this TBI mouse model are ongoing to distinguish between acute

versus chronic late impacts of radiation damage on ovarian function and to determine whether the mechanisms of iatrogenic and physiologic reproductive aging are similar or distinct. Furthermore, it is important to acknowledge that in the TBI model, we can not readily distinguish whether the observed follicle loss is due to direct damage to the ovary or instead due to indirect systemic or abscopal effects. Using the Small Animal Radiation Research Platform, we compared the effects of targeted radiation vs. total body irradiation on the ovary following a single 1 Gy dose (Grover et al, under review). We found that at 2 weeks post-exposure, there was no significant difference between the ovarian damage elicited by direct versus indirect effects, suggesting that, at least in the short-term, there are negligible compounding systemic effects on the ovary.

Supplementary Material

Refer to Web version on PubMed Central for supplementary material.

Acknowledgments

We would like to thank Jing Huang (KUMC Histology Core) and Megan Larmore (University of Washington Histology and Imaging Core) for their technical assistance in ovarian tissue sectioning and quantitative microscopy analysis, respectively.

Funding

This work was supported by the Center for Reproductive Health After Disease (P50 HD076188 to F.E.D.) from the National Centers for Translational Research in Reproduction and Infertility (NCTRI). The KUMC Histology Core was supported by the P30 HD002528 (Kansas IDDRC).

References

Adriaens I, Smitz J, Jacquet P. The current knowledge on radiosensitivity of ovarian follicle development stages. Hum Reprod Update. 2009; 15:359–377. [PubMed: 19151106]

Baker TG. Effects of ionizing radiations on mammalian oogenesis: a model for chemical effects. Environ Health Perspect. 1978; 24:31–37. [PubMed: 17539151]

Briley SM, Jasti S, McCracken JM, Hornick JE, Fegley B, Pritchard MT, Duncan FE. Reproductive age-associated fibrosis in the stroma of the mammalian ovary. Reproduction. 2016; 152:245–260. [PubMed: 27491879]

Bristol-Gould SK, Kreeger PK, Selkirk CG, Kilen SM, Cook RW, Kipp JL, Shea LD, Mayo KE, Woodruff TK. Postnatal regulation of germ cells by activin: the establishment of the initial follicle pool. Dev Biol. 2006; 298:132–148. [PubMed: 16930587]

Broekmans FJ, Soules MR, Fauser BC. Ovarian aging: mechanisms and clinical consequences. Endocr Rev. 2009; 30:465–493. [PubMed: 19589949]

Critchley HO, Wallace WH. Impact of cancer treatment on uterine function. J Natl Cancer Inst Monogr. 2005:64–68. [PubMed: 15784827]

Duncan FE, Jasti S, Paulson A, Kelsh JM, Fegley B, Gerton JL. Age-associated dysregulation of protein metabolism in the mammalian oocyte. Aging Cell. 2017; 16:1381–1393. [PubMed: 28994181]

Grigsby PW, Russell A, Bruner D, Eifel P, Koh WJ, Spanos W, Stetz J, Stitt JA, Sullivan J. Late injury of cancer therapy on the female reproductive tract. Int J Radiat Oncol Biol Phys. 1995; 31:1281–1299. [PubMed: 7713788]

Hutt KJ. The role of BH3-only proteins in apoptosis within the ovary. Reproduction. 2014

Kerr JB, Brogan L, Myers M, Hutt KJ, Mladenovska T, Ricardo S, Hamza K, Scott CL, Strasser A, Findlay JK. The primordial follicle reserve is not renewed after chemical or gamma-irradiation mediated depletion. Reproduction. 2012a; 143:469–476. [PubMed: 22301887]

Kerr JB, Hutt KJ, Michalak EM, Cook M, Vandenberg CJ, Liew SH, Bouillet P, Mills A, Scott CL, Findlay JK, Strasser A. DNA damage-induced primordial follicle oocyte apoptosis and loss of fertility require TAp63-mediated induction of Puma and Noxa. Mol Cell. 2012b; 48:343–352. [PubMed: 23000175]

Meirow D, Biederman H, Anderson RA, Wallace WH. Toxicity of chemotherapy and radiation on female reproduction. Clin Obstet Gynecol. 2010; 53:727–739. [PubMed: 21048440]

Morita Y, Perez GI, Paris F, Miranda SR, Ehleiter D, Haimovitz-Friedman A, Fuks Z, Xie Z, Reed JC, Schuchman EH, Kolesnick RN, Tilly JL. Oocyte apoptosis is suppressed by disruption of the acid sphingomyelinase gene or by sphingosine-1-phosphate therapy. Nat Med. 2000; 6:1109–1114. [PubMed: 11017141]

Nicholson DW, Ali A, Thornberry NA, Vaillancourt JP, Ding CK, Gallant M, Gareau Y, Griffin PR, Labelle M, Lazebnik YA, et al. Identification and inhibition of the ICE/CED-3 protease necessary for mammalian apoptosis. Nature. 1995; 376:37–43. [PubMed: 7596430]

Rinaldi VD, Hsieh K, Munroe R, Bolcun-Filas E, Schimenti JC. Pharmacological Inhibition of the DNA Damage Checkpoint Prevents Radiation-Induced Oocyte Death. Genetics. 2017; 206:1823–1828. [PubMed: 28576861]

Sanders JE, Hawley J, Levy W, Gooley T, Buckner CD, Deeg HJ, Doney K, Storb R, Sullivan K, Witherspoon R, Appelbaum FR. Pregnancies following high-dose cyclophosphamide with or without high-dose busulfan or total-body irradiation and bone marrow transplantation. Blood. 1996; 87:3045–3052. [PubMed: 8639928]

Scholzen T, Gerdes J. The Ki-67 protein: from the known and the unknown. J Cell Physiol. 2000; 182:311–322. [PubMed: 10653597]

Straub JM, New J, Hamilton CD, Lominska C, Shnayder Y, Thomas SM. Radiation-induced fibrosis: mechanisms and implications for therapy. J Cancer Res Clin Oncol. 2015; 141:1985–1994. [PubMed: 25910988]

Wallace WH, Shalet SM, Crowne EC, Morris-Jones PH, Gattamaneni HR. Ovarian failure following abdominal irradiation in childhood: natural history and prognosis. Clin Oncol (R Coll Radiol). 1989; 1:75–79. [PubMed: 2486484]

Wallace WH, Thomson AB, Kelsey TW. The radiosensitivity of the human oocyte. Hum Reprod. 2003; 18:117–121. [PubMed: 12525451]

Weintraub NL, Jones WK, Manka D. Understanding radiation-induced vascular disease. J Am Coll Cardiol. 2010; 55:1237–1239. [PubMed: 20298931]

Wo JY, Viswanathan AN. Impact of radiotherapy on fertility, pregnancy, and neonatal outcomes in female cancer patients. Int J Radiat Oncol Biol Phys. 2009; 73:1304–1312. [PubMed: 19306747]

Yu J, Hecht NB, Schultz RM. RNA-binding properties and translation repression in vitro by germ cell-specific MSY2 protein. Biol Reprod. 2002; 67:1093–1098. [PubMed: 12297523]

Zelinski MB, Murphy MK, Lawson MS, Jurisicova A, Pau KY, Toscano NP, Jacob DS, Fanton JK, Casper RF, Dertinger SD, Tilly JL. In vivo delivery of FTY720 prevents radiation-induced ovarian failure and infertility in adult female nonhuman primates. Fertil Steril. 2011; 95:1440–1445. e1441–1447. [PubMed: 21316047]

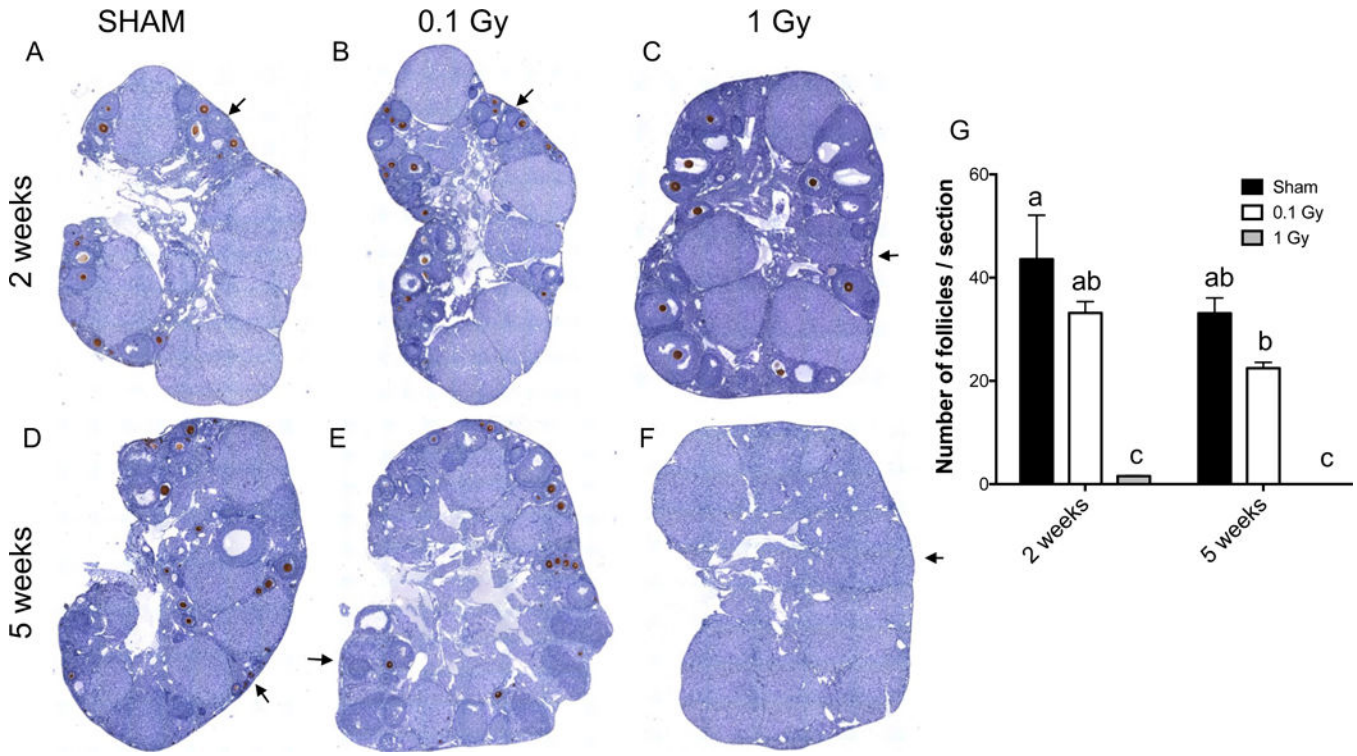

Figure 1. A single dose of 1 Gy TBI depletes total follicle numbers by 2 weeks post-exposure

Histologic sections of ovarian tissue from (A, D) control sham mice and mice exposed to a single dose of (B, E) 0.1 Gy or (C, F) 1 Gy that were harvested either (A-C) 2 weeks or (D-F) 5 weeks post-exposure were stained with the oocyte-specific MSY2 antibody (brown, DAB) and counterstained with hematoxylin. Representative images are shown. (G) Follicle numbers in all follicle classes were quantified for each cohort and reported as the average number of follicles per section per ovary. The different letters denote a statistically significant difference between groups as assessed by a two-way ANOVA ($P \leq 0.01$). The regions highlighted by the arrow are further magnified in Figure 2.

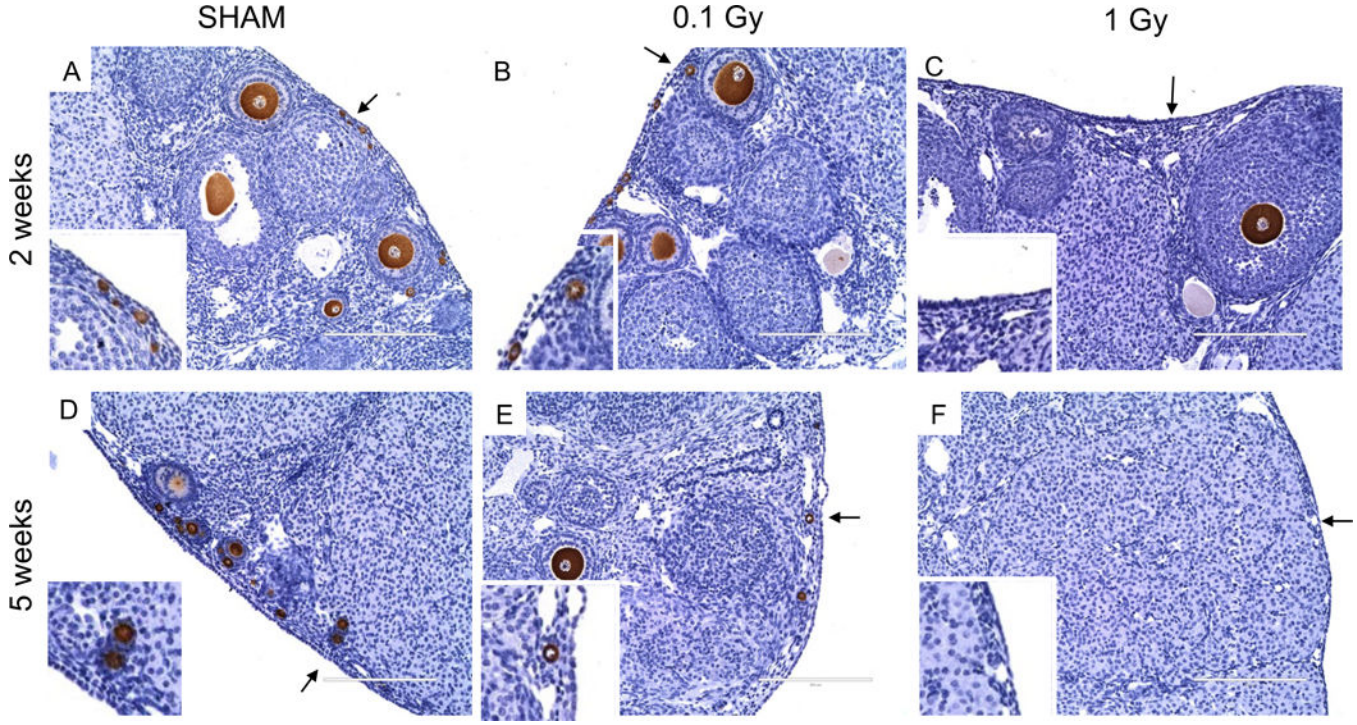

Figure 2. Histologic analysis demonstrates that primordial and primary follicles are absent in the ovarian cortex following exposure to a single dose of 1 Gy radiation

(A-F) show magnified images of the ovary in the corresponding regions highlighted in Figure 1. The insets show specific regions of the ovarian cortex that are marked by the arrows. These images illustrate the significant follicle damage that occurs in response to a single dose of 1 Gy radiation at both 2 weeks and 5 weeks post-exposure. Note the clear lack of primordial and primary follicles in both (C) and (F). In addition, large growing follicles are only observed at 2 weeks post-exposure to 1 Gy (C) and not at 5 weeks (F). Scale bars are 200 μm.

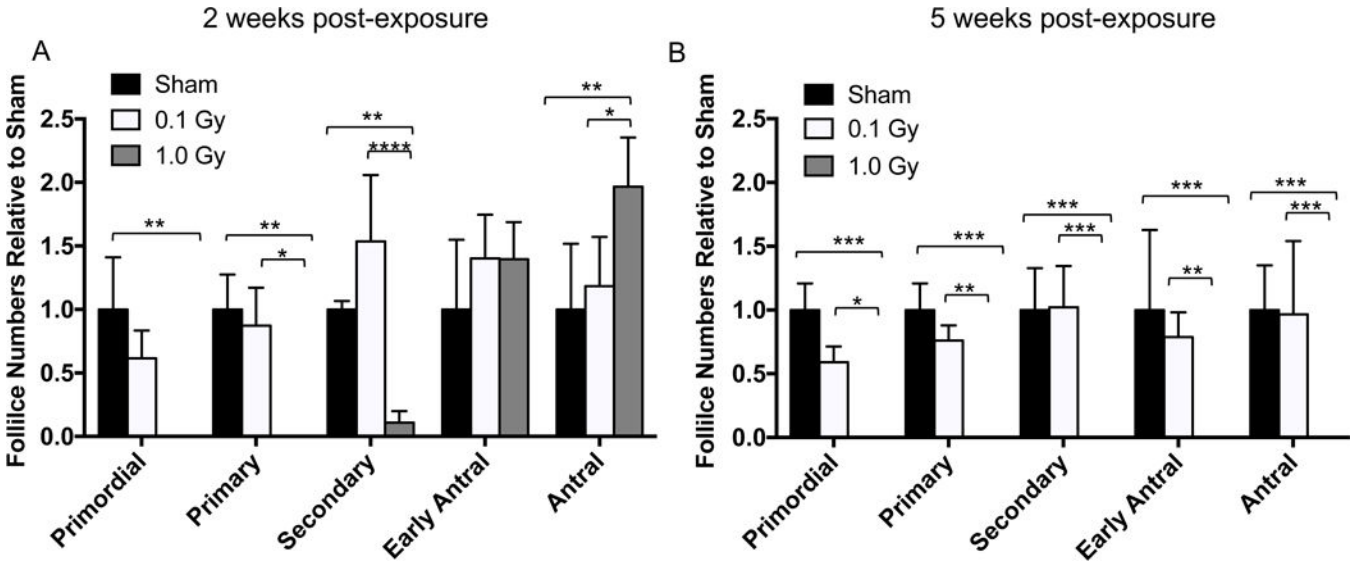

Figure 3. Stage-dependent differences in ovarian follicle numbers occur in response to single doses of 0.1 and 1 Gy TBI

Follicle stages were classified and counted for each experimental cohort (sham, 0.1 Gy, and 1 Gy), and the average follicle numbers per section in each class were expressed relative to the average number of follicles in the sham controls at (A) two weeks and (B) five weeks post-exposure. Statistically significant differences between the groups were assessed by a two-way ANOVA, and asterisks highlight significant differences (*P ≤ 0.05, ** P ≤ 0.01, *** P ≤ 0.001, **** P ≤ 0.0001). Of note, in the 1 Gy cohort (gray bars), only growing follicles remained at 2 weeks but no follicles were observed at 5 weeks.

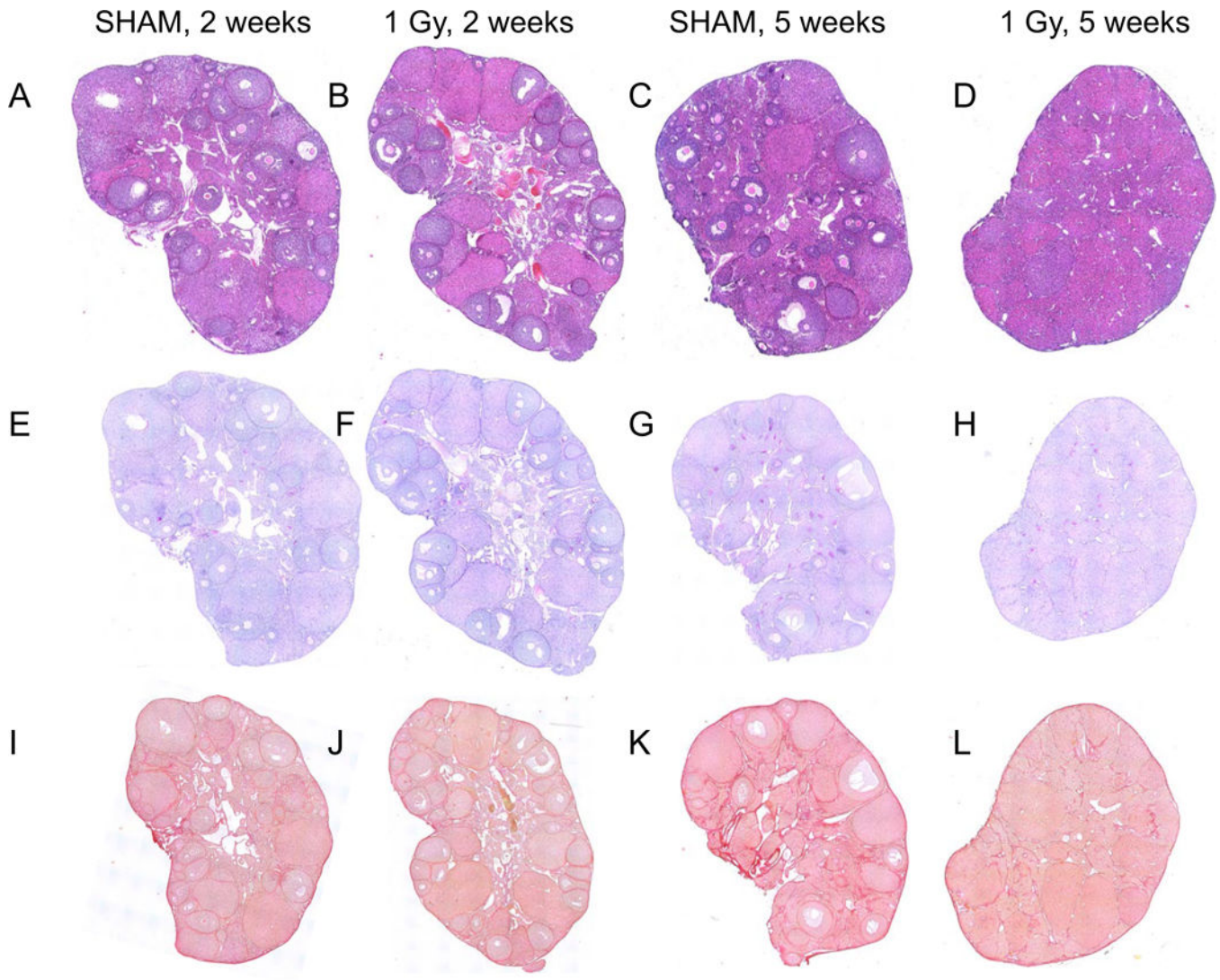

Figure 4. Histologic stains reveal healthy ovarian stromal tissue following a single dose exposure to 1 Gy TBI at 2 and 5 weeks post-exposure

Ovaries from (A, C, E, G, I, K) sham mice or (B, D, F, H, J, L) mice exposed to 1 Gy radiation were harvested either two weeks (left two image columns) or five weeks (right two image columns) post-exposure and histologic sections were stained for (A-D) general architecture (hematoxylin and eosin), (E-H) polysaccharides (Periodic Acid Schiff), and (I-L) collagen I/III (Picrosirius Red). Representative images are shown.

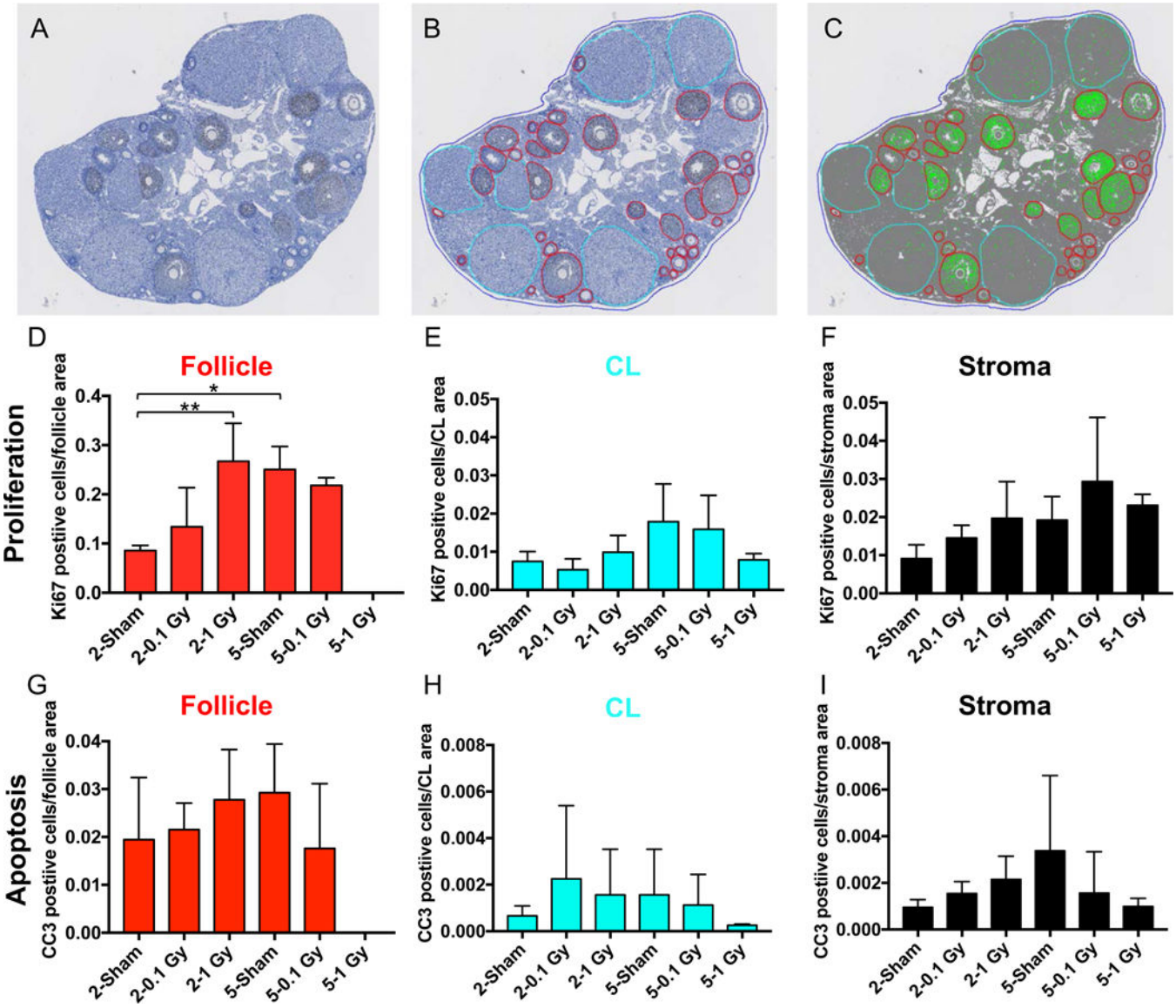

Figure 5. The ovarian stroma does not exhibit changes in cell proliferation or cell death in response to single doses of 0.1 and 1 Gy TBI at 2 and 5 weeks post-exposure

(A) Ovarian tissue sections were stained with an antibody against the cell proliferation marker, Ki67, using automated immunohistochemistry and whole slides were imaged. Quantitative microscopy was performed using Visiopharm software where (B) regions of interest (follicle – red, corpora lutea; CL- cyan, ovarian area – blue) were manually defined. (C) The Visiopharm software was trained to label and count positive (brown DAB) and background tissue counterstain (hematoxylin, blue) using a project specific configuration based on a threshold of pixel values (green). The same analyses shown in (A-C) were done for histologic sections stained with the apoptosis marker CC3. Validation of these antibodies are shown in Supplemental Figure 4. Using this approach, we were able to quantify the number of (D-F) proliferating or (G-I) apoptotic cells per specific ovarian area, including (D, G) the follicle, (E, H) the CL, and (F, I) the stroma. The stromal area was defined as the [total ovarian area – (follicle area + CL area)]. Statistically significant differences between

the groups were assessed by a one-way ANOVA, and asterisks highlight significant differences (*P ≤ 0.05, ** P ≤ 0.01). Follicles were completely absent in the 1 Gy cohort at 5 weeks, hence there was no proliferation or apoptosis noted in this ovarian compartment.

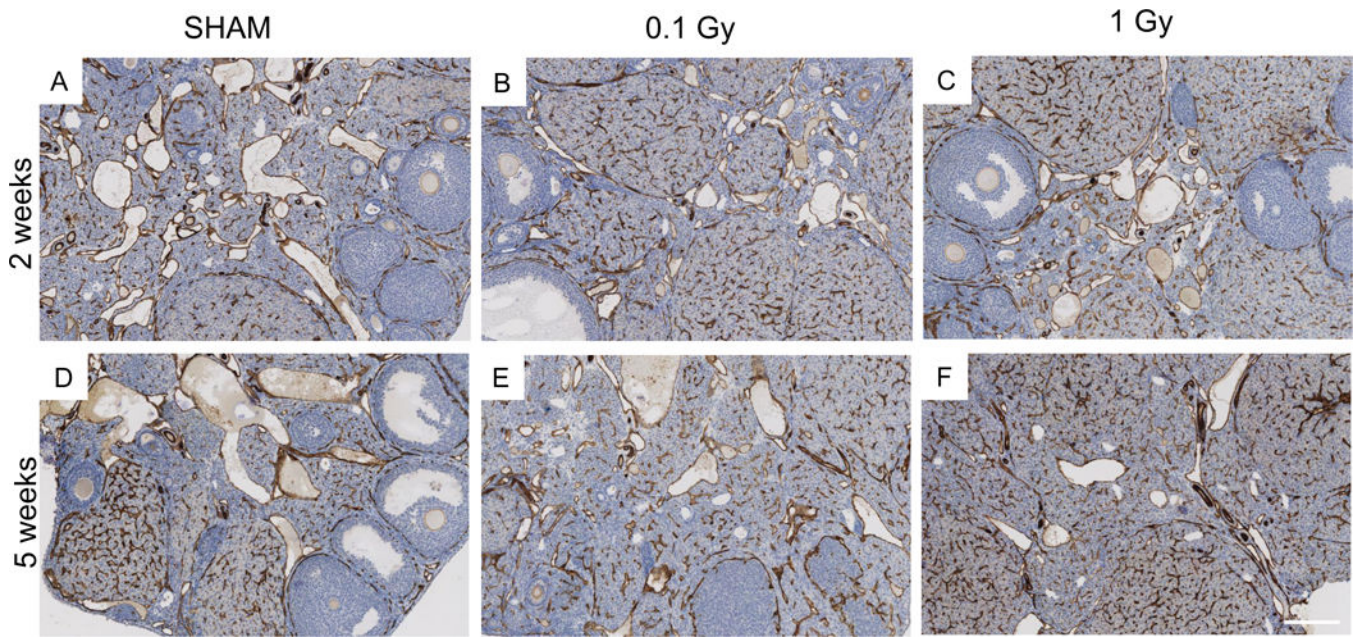

Figure 6. The ovarian vasculature does not undergo prominent architectural changes in response to single doses of 0.1 and 1 Gy TBI at 2 and 5 weeks post-exposure

Ovaries from (A, D) sham mice or mice exposed to (B, E) 0.1 Gy or (C, F) 1 Gy radiation were harvested either two weeks (A-C) or five weeks (D-F) post-exposure and histologic sections were processed for automated immunohistochemistry (IHC) with an antibody against the endothelial cell marker CD31. The validation for the use of this antibody for IHC is shown in Supplemental Figure 4. Representative images are shown. The scale bar is 200 μm.